Supporting Information

Optical characterization of silicon nitride metagrating-based lightsails for self-stabilization

Ramon Gao[1], Michael D. Kelzenberg[1], Yonghwi Kim[1], Ognjen Ilic[2], Harry A. Atwater[1]*

1. Thomas J. Watson Laboratories of Applied Physics, California Institute of Technology, Pasadena, CA 91125, USA
2. Department of Mechanical Engineering, University of Minnesota, Minneapolis, MN 55455, USA

*E-mail: haa@caltech.edu

Contents: (9 pages)

S1. Fabrication of silicon nitride metagratings

Fabrication of silicon nitride metagratings is summarized in Figure S1 and started with low stress (< 250 MPa) silicon nitride membranes purchased from Norcada (NX10100D, 200 nm thickness, 1 mm x 1 mm window size, 10 mm x 10 mm frame size, 200 µm frame thickness). We spin-coated a positive-tone diluted resist (ZEP 520A, D.R. 1.5) at a rotation speed of 1500 rpm for 1 minute onto the membrane to obtain an approximately 280 nm thick resist layer. To prevent the window from being broken by the vacuum chuck of the spin-coater, we mounted the chip onto the chuck holder at one of the chip's corners. We experimented with different mounting approaches, including gluing the chip to a second carrier chip and taping the chip to a glass slide, however, surprisingly, we found that the asymmetric mounting approach produced the most uniform resist films. After baking the resist on a hot plate at 180°C for 5 minutes, a conductive polymer layer acting as an antistatic agent for electron beam lithography (aquaSAVE) was spin-coated on top of the resist (1500 rpm for 1 minute). Patterns were defined using electron beam lithography (100 kV, 0.3 nA beam current, 280 µC/cm^2 exposure dose). Afterwards, the polymer layer was removed by immersing the chip into deionized (DI) water, and developed in ZED-N50 for 2 minutes and 30 seconds. We then cleaned the chip in isopropyl alcohol (IPA), and dried it by gently blowing it dry with a nitrogen gun.

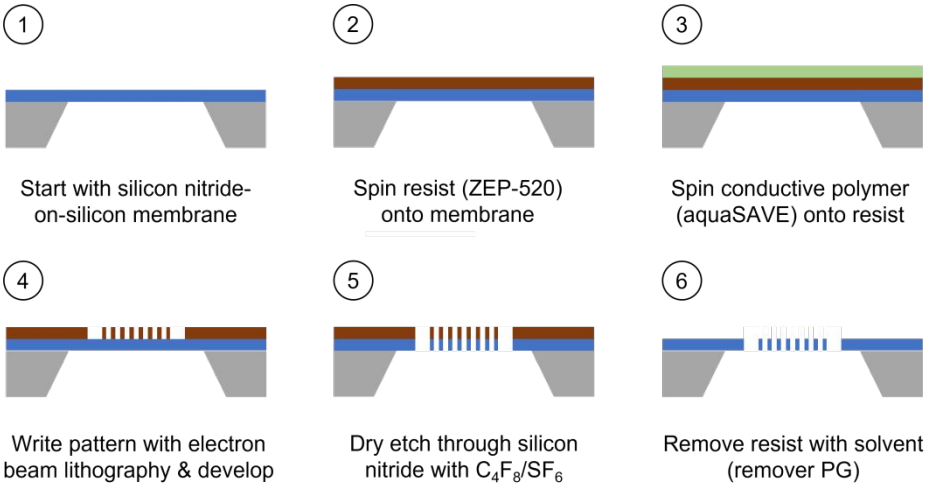

Figure S1: Fabrication steps from a commercial silicon nitride membrane to a self-stabilizing metagrating.

For the pattern transfer via inductive-coupled plasma reactive ion etching, we fixed the chip onto a silicon carrier wafer using a viscous thermal oil (Santovac). Our etch recipe is based on SF_6 (38 sccm) as the etchant gas and C_4F_8 (52 sccm) as the passivation gas. After an etch time of 5 minutes, we carefully removed the chip from the carrier wafer, making sure that the etched silicon nitride window did not get contaminated by the thermal oil, and removed the remaining oil from the backside of the chip with acetone. We immersed our sample vertically into multiple baths (5) of heated (~ 70°C) remover PG for 30 minutes to strip the resist layer, before cleaning off

remaining scum and residues with two 10 min long baths in IPA followed by two 5 min long baths in DI water. Finally, the chip was carefully dried using a nitrogen gun, and inspected visually using an optical microscope for visible defects and residues prior to measurements.

S2. Calculation of optical forces and torques from measured scattering

Sections 2 and 3 closely follow theory presented by Ilic and Atwater[1]. After measuring the normalized intensities (reflection and transmission coefficients) r_m and t_m of reflected and transmitted diffraction orders, respectively, and their diffraction angles β_m for $m = 0, \pm 1$, as presented in the main text, we calculated the optically induced pressure on the *left* half of the self-stabilizing metagrating-based lightsail using the photon momentum balance equation

$$\boldsymbol{p}^L = -\frac{I}{c}\left(\boldsymbol{e_z} + \sum_{m=-1}^{+1}[t_m \sin(\beta_m - \theta) + r_m \sin(\beta_m + \theta)]\boldsymbol{e_x} + [-t_m \cos(\beta_m - \theta) + r_m \cos(\beta_m + \theta)]\boldsymbol{e_z}\right),$$

Noting that $\boldsymbol{p}^L$ inferred from measurements of optical scattering is defined in the inertial (laboratory) frame.

The optically induced force per unit depth in *y*-direction on the *left* half of the lightsail is then given by

$$F^L_{x,z}(x,\theta) = \int_0^{D/2} ds \cos(\theta) p^L_{x,z}(\theta) e^{-2(x + s\cos(\theta))^2/w^2} = -\frac{w}{2}\sqrt{\frac{\pi}{2}}\left(\mathrm{erf}\left(\frac{\sqrt{2}x}{w}\right) - \mathrm{erf}\left(\frac{2x + D\cos(\theta)}{\sqrt{2}w}\right)\right) p^L_{x,z},$$

Assuming an incident beam of Gaussian shape with beam waist w, whose intensity profile is described by

$$I(x) = I_0 e^{-2x^2/w^2}.$$

Due to the mirror-symmetric arrangement of unit cells within left and right halves, we can directly calculate the total optical force on both halves in the body frame as

$$F_x(x,\theta) = F^L_x(x,\theta) + F^R_x(x,\theta) = F^L_x(x,\theta) - F^L_x(-x,-\theta),$$

$$F_z(x,\theta) = F^L_z(x,\theta) + F^R_z(x,\theta) = F^L_z(x,\theta) + F^L_z(-x,-\theta).$$

The optically induced in-plane torque per unit depth in the *y*-direction can be expressed as

$$\tau_y(x,\theta) = \int_0^{D/2} ds \cos(\theta) s\left[-\sin(\theta) p^L_x(\theta) - \cos(\theta) p^L_z(\theta)\right] e^{-2(x + s\cos(\theta))^2/w^2} + \int_0^{D/2} ds \cos(\theta) s \left[\sin(\theta) p^R_x(\theta) + \cos(\theta) p^R_z(\theta)\right] e^{-2(x - s\cos(\theta))^2/w^2},$$

With

$$p^R_x(\theta) = -p^L_x(-\theta),$$

$$p_z^R(\theta) = p_z^L(-\theta).$$

Instead of expressing the torque in terms of optical pressures defined in the inertial frame, one can equivalently calculate $\tau_y(x,\theta)$ as

$$\tau_y(x,\theta) = \int_0^{D/2} ds\cos(\theta)s\left[-p_z^{L,\mathrm{BF}}(\theta)\right]e^{-2(x+s\cos(\theta))^2/w^2} + \int_0^{D/2} ds\cos(\theta)s\left[p_z^{R,\mathrm{BF}}(\theta)\right]e^{-2(x-s\cos(\theta))^2/w^2},$$

As the pressure can converted between the body frame and inertial frame via

$$\boldsymbol{p}^{\mathrm{BF}} = \begin{pmatrix}\cos(\theta) & -\sin(\theta)\\ \sin(\theta) & \cos(\theta)\end{pmatrix}\boldsymbol{p} = \begin{pmatrix}p_x^L\cos(\theta) - p_z^L\sin(\theta)\\ p_x^L\sin(\theta) + p_z^L\cos(\theta)\end{pmatrix}.$$

We have to make several assumptions as we evaluate the integrals above: (1) an approximately non-varying beam intensity across the element ds, i.e., $w \gg ds$, (2) sufficiently many unit cells within ds such that $ds \gg d$. Given the chosen beam width of $w = 2D$, with the stated assumptions, we automatically ensure that $D \gg d$ holds, such that the contribution to the torque is dominated by the radiation pressure force.

S3. Calculation of Jacobian matrix from equations of motion

The equations of motion for a lightsail in two dimensions are given by

$$m\frac{d^2z}{dt^2} \approx F_z(x,\theta),$$

$$m\frac{d^2x}{dt^2} = F_x(x,\theta),$$

$$I\frac{d^2\theta}{dt^2} = \tau_y(x,\theta),$$

Where we neglect the effect of gravity in the radiation pressure dominated regime, and with m being the mass of the structure per unit depth in y-direction, $I = \gamma mD^2$ the moment of inertia with respect to the lightsail's center of mass, and $\gamma = 1/12$ given rotation around the y-axis. By introducing normalized, i.e., unitless variables, we can rewrite the equations of motion as scaled equations

$$\frac{d^2z'}{dt'^2} \approx f_{z'}(x',\theta),$$

$$\frac{d^2x'}{dt'^2} = f_{x'}(x',\theta),$$

$$\frac{d^2\theta}{dt'^2} = f_\theta(x',\theta),$$

With dimensionless pressures $p' = (c/I_0)p$, lengths $x' = x/D$ and time $t' = t/(mc/I_0)^{1/2}$.

From here on (dropping the primed notation), it is convenient to express the scaled equations of motion in vector form

$$\frac{d\mathbf{u}}{dt} = \mathbf{f}(\mathbf{u}),\ \mathbf{u} = (x,\theta,v,\omega)^T,\ \mathbf{f} = (v,\omega,f_x,f_\theta)^T,$$

With $\mathbf{u}_0 = \mathbf{0}$ being an equilibrium point given that $\mathbf{f}(\mathbf{u}_0) = \mathbf{0}$. Consequently, the Jacobian matrix of the vectorial first-order differential equation is calculated as

$$\mathbf{f}'(\mathbf{u}_0) = \begin{bmatrix} 0 & 0 & 1 & 0 \\ 0 & 0 & 0 & 1 \\ f_{xx} & f_{x\theta} & 0 & 0 \\ f_{\theta x} & f_{\theta\theta} & 0 & 0 \end{bmatrix}\Bigg|_{\mathbf{u}_0},$$

With the four partial derivatives $f_{ij} = \partial f_i/\partial j$. Its four eigenvalues are then given by

$$\Lambda_{1-4} = \pm\frac{1}{\sqrt{2}}\sqrt{f_{xx} + f_{\theta\theta} \pm \sqrt{(f_{xx} - f_{\theta\theta})^2 + 4f_{\theta x}f_{x\theta}}}.$$

For the simulated design, we numerically evaluated the eigenvalues to $\Lambda_{1,3} \approx \pm 0.52i$ and $\Lambda_{2,4} \approx \pm 1.63i$.

S4. Fitting r_0 for small incidence angles

Due to the inherent inability of our setup to measure the specularly reflected order for small incidence angles θ, we fitted the recorded intensities of r_0 at larger θ to a parabolic function based on its expected functional dependence on θ as observed from simulations. The fitted parameters of the parabolic function $r_0(\theta) = a\theta^2 + b\theta + c$ shown in Figure S2 are given by a = 0.000583 ± 0.0000096, b = 0.000035 ± 0.0000299 and c = 0.048626 ± 0.0006423. We then completed the measured data range for r_0 with the fitted values in the range from −5° to 4°.

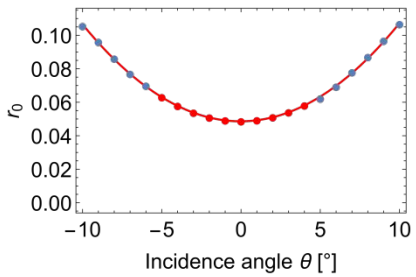

Figure S2: Fitted intensity of measured specularly reflected order (blue dots) with a parabolic function (red curve), from which we sampled the missing intensities at small incidence angles θ (red dots).

S5. Beam characterization

To characterize the shape and size of the beam focused onto the sample, we placed a CMOS camera sensor in the beam focus of the specimen plane of our experimental apparatus, producing the image shown in Figure S3a. Ensuring that no pixel (size 2.4 µm x 2.4 µm) was overexposed, we can plot the beam intensity along x and y with the origin being at the maximum intensity of the beam as seen in Figure S3b and S3c. We find that the beam is slightly elongated along y, but is otherwise substantially contained within our metagrating device of size 120 µm x 120 µm, as we determine the full width at half maximum of the focused laser spot to be ~ 60 µm along y and ~ 50 µm along x. Therefore, we can make the assumption that the measured optical response from our sample stems from the metagrating itself and that effects from the edges of the metagrating can be neglected. To further verify this and quantify the effect of a finite size beam instead of the assumed plane wave in simulations, we have also convolved measured reflection and transmission coefficients with a Gaussian kernel of beam width 30 µm, and found that the results are practically indiscernible from the data prior to convolution.

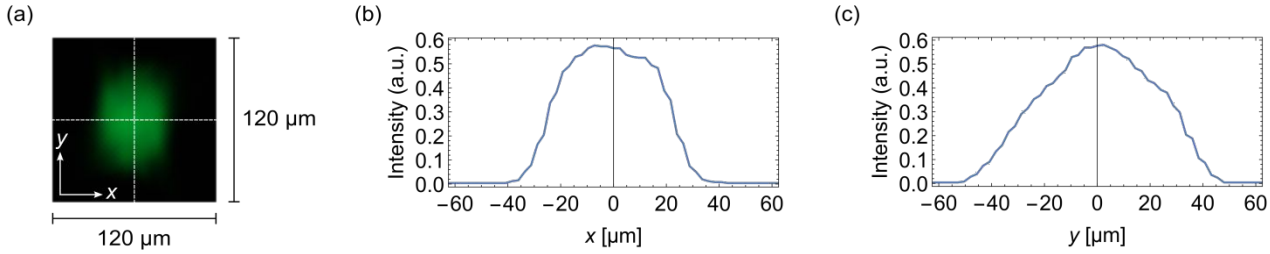

Figure S3: (a) Image of the focused beam being mostly contained within the metagrating device of size 120 µm x 120 µm, with cuts showing the intensity profile (b) along the horizontal direction x and (c) the vertical direction y.

S6. Error propagation analysis

To quantify the effect of a finite-size photodetector, scattering from the mechanically supporting anchor bars, measurement uncertainties and fabrication imperfections on the inferred passive stabilization mechanism of the reported metagratings, we performed the following error propagation analysis. As stated in the main text, we assumed that the normalized diffraction order intensities (reflection and transmission coefficients) were measured with an absolute uncertainty of ±0.01, whereas we assigned an absolute standard error of ±1° to the diffraction

angles $\Delta\beta_{\pm 1}$ due to the peak fitting and subsequent Gaussian filtering procedure on the raw data. Due to the setup-related inability to measure r_0 at small incidence angles θ, we attributed a larger standard error of ±0.05 to r_0. On the other hand, the uncertainty associated with the incidence angle θ can be narrowed down due to our two-step alignment process. To ensure that $\theta = 0°$ corresponds to when the focused laser beam is normal to the sample surface, we first adjusted the tilt of the sample rotation stage such that the specularly reflected light lined up vertically with the incident beam on the objective. Following this coarse alignment approach, we then measured the optical response of a non-blazed symmetrically diffracting grating fabricated on the same chip. The stage tilt at which t_{-1} and t_{+1} are equal corresponds to $\theta = 0°$, allowing us to determine θ with a lower uncertainty of ~0.1°. Therefore, with

$$\Delta r_{\pm 1} = \Delta t_{0,\pm 1} = 0.01,\ \Delta r_0 = 0.05,$$

$$\Delta\beta_{\pm 1} \equiv \Delta\beta = 1°,\ \Delta\theta = 0.1°,$$

We can propagate these assumed uncertainties to the optically induced pressure by calculating

$$\Delta p_x^L \approx \sqrt{\left(\frac{\partial p_x^L}{\partial\theta}\Delta\theta\right)^2 + \left(\sum_{m=\{-1,+1\}}\left(\frac{\partial p_x^L}{\partial\beta_m}\Delta\beta\right)^2 + \left(\frac{\partial p_x^L}{\partial t_m}\Delta t_m\right)^2\right) + \left(\sum_{m=-1}^{+1}\left(\frac{\partial p_x^L}{\partial r_m}\Delta r_m\right)^2\right)},$$

$$\Delta p_z^L \approx \sqrt{\left(\frac{\partial p_z^L}{\partial\theta}\Delta\theta\right)^2 + \left(\sum_{m=\{-1,+1\}}\left(\frac{\partial p_z^L}{\partial\beta_m}\Delta\beta\right)^2\right) + \left(\sum_{m=-1}^{+1}\left(\frac{\partial p_z^L}{\partial r_m}\Delta r_m\right)^2 + \left(\frac{\partial p_z^L}{\partial t_m}\Delta t_m\right)^2\right)}.$$

To calculate the partial derivatives of the pressures with respect to all parameters, we fit $p_{x,z}^L$ to an approximate function by interpolating the data points. While the whole range of measured incidence angles between −10° and 10° was used to calculate the Jacobian and eigenvalues reported in the main text, for this analysis, we limited the propagation of errors to reflection and transmission coefficients at $\theta = 0°, \pm 1°$. Therefore, the maximum sensible order of the fit is 2, which corresponds to a quadratic function.

With this approach, we calculated the normalized optical pressures along with their uncertainties to be

$$p_x^L(-1°) = 0.260698 \pm 0.015827 = -p_x^R(1°),$$

$$p_x^L(0°) = 0.267727 \pm 0.015946 = -p_x^R(0°),$$

$$p_x^L(1°) = 0.272829 \pm 0.016215 = -p_x^R(-1°),$$

$$p_z^L(-1°) = -1.04645 \pm 0.052989 = p_z^R(1°),$$

$$p_z^L(0°) = -1.03172 \pm 0.052967 = p_z^R(0°),$$

$$p_z^L(1°) = -1.0067 \pm 0.05290 = p_z^R(-1°).$$

From here on, we sampled 10^6 times from the normally distributed pressures with their means and standard errors (σ) at $\theta = 0°, \pm 1°$ given above, and then calculated the resulting 10^6 distinct Jacobians and their eigenvalues. Out of this set of a million samples, ~ 58.43% of Jacobians had purely imaginary eigenvalues.

To verify this approach of propagating standard errors from measured data to derived pressures, followed by a Monte Carlo sampling to provide an uncertainty to the dynamical stability inferred from measurements, we have also sampled $r_{0,\pm1}$, $t_{0,\pm1}$, $\beta_{\pm1}$ and θ directly 10^6 times according to their normal distributions defined by their measured values and the assumed standard errors. By calculating the corresponding 10^6 different values for p_x and p_z at $\theta = 0°, \pm 1°$, and evaluating the Jacobians along with their eigenvalues, we found that ~ 58.53% of sampled cases produced pure imaginary eigenvalues, which converges to the result from our initial approach. For this full Monte Carlo sampling approach, we can further neglect cases where $\sum_i (r_i + t_i) \geq 1$, which results in a slightly increased percentage of marginally stable cases of 59.14%.

Finally, we note that although the equations for optical pressures in the main text do not take diffusive scattering and out-of-plane diffraction into account, our error analysis indirectly and partly accounts for these effects due to the uncorrelated variations of all scattered intensities.

References

(1) Ilic, O.; Atwater, H. A. Self-Stabilizing Photonic Levitation and Propulsion of Nanostructured Macroscopic Objects. *Nat. Photonics* **2019**, *13* (4), 289–295. https://doi.org/10.1038/s41566-019-0373-y.